

Article

# Selectivity Regulation of Au/Titanate by Biochar Modification for Selective Oxidation of Benzyl Alcohol

Xiya Chen <sup>1</sup>, Hangwei Jiang <sup>1</sup>, Danlan Cui <sup>1</sup>, Kun Lu <sup>1</sup>, Xiao Kong <sup>1</sup>, Junmeng Cai <sup>2</sup>, Shirui Yu <sup>3,4</sup> and Xingguang Zhang <sup>1,\*</sup> 

<sup>1</sup> School of Materials and Chemistry, University of Shanghai for Science and Technology, 516 Jungong Road, Shanghai 200093, China

<sup>2</sup> Biomass Energy Engineering Research Center, School of Agriculture and Biology, Shanghai Jiao Tong University, 800 Dongchuan Road, Shanghai 200240, China

<sup>3</sup> Department of Food Science and Engineering, Moutai Institute, Luban Street, Renhuai 564502, China

<sup>4</sup> Guizhou Health Wine Brewing Technology Engineering Research Center, Moutai Institute, Luban Street, Renhuai 564502, China

\* Correspondence: x.g.zhang@usst.edu.cn

**Abstract:** In organic synthesis, it is important to control the selectivity target product with high purity and reduce the cost of energy and equipment for separation. This study investigated supported gold catalysts on biochar-modified titanate-based nanofibers in order to regulate the catalytic performances by biochar content and surface properties. The catalysts were characterized by SEM, TEM, XRD, XPS, ICP-OES, UV-Vis to confirm their morphology, particle size distribution of Au NPs, crystal structures, oxidation state of Au and other key elements, real Au loading, and optical properties. In the test of selective oxidation of benzyl alcohol to benzaldehyde, the biochar modification could improve the selectivity toward benzaldehyde. Moreover, the influence of catalyst calcination conditions, reaction time, reaction atmospheres, reaction temperatures and solvent were systematically investigated. These results are useful for peer researchers in rational catalyst design.

**Keywords:** gold catalysts; selectivity regulation; selective oxidation; benzyl alcohol



**Citation:** Chen, X.; Jiang, H.; Cui, D.; Lu, K.; Kong, X.; Cai, J.; Yu, S.; Zhang, X. Selectivity Regulation of Au/Titanate by Biochar Modification for Selective Oxidation of Benzyl Alcohol. *Catalysts* **2023**, *13*, 864. <https://doi.org/10.3390/catal13050864>

Academic Editor: Evangelos Topakas

Received: 13 March 2023

Revised: 4 May 2023

Accepted: 8 May 2023

Published: 10 May 2023



**Copyright:** © 2023 by the authors. Licensee MDPI, Basel, Switzerland. This article is an open access article distributed under the terms and conditions of the Creative Commons Attribution (CC BY) license (<https://creativecommons.org/licenses/by/4.0/>).

## 1. Introduction

In organic synthesis, selective oxidation of organic compounds (e.g., alcohols) is an important process in industries, such as agrochemicals, pharmaceuticals, petrochemicals, plastics, pesticides, and dyes [1,2]. These oxidation reactions are usually consecutive and/or in parallel (namely side reactions) and thus necessitate highly selective catalysts to control the reaction processes without leading to complete oxidation or unwanted reactions. The selective oxidation of benzyl alcohol to benzaldehyde is usually a model reaction for developing and designing heterogeneous catalysts, and benzaldehyde is industrially produced by hydrolysis of benzyl chloride, selective oxidation toluene, or selective hydrogenation of aromatic ester, leading to a large number of by-products and environmental pollution [3,4].

In heterogeneous catalysis, the approaches to reducing side reactions for selective oxidation of benzyl alcohol include utilization of green and clean oxidants (e.g., air and O<sub>2</sub>), photocatalytic processes under ambient reaction conditions, solvent-free processes, and mostly choice of appropriate heterogeneous catalysts. Supported metal or alloy catalysts are popular for selective oxidation of benzyl alcohol, of which gold-based catalysts are important research areas. Gold nanoparticles (Au NPs) have excellent catalytic activity in the selective oxidation of benzyl alcohol as reported in many studies [5,6], and the catalytic performances of supported noble metal catalysts can be significantly improved by selecting appropriate support materials, preparation methods, and combinations with other metals [7,8]. Some regular supports, such as carbon [9], TiO<sub>2</sub> [10], Al<sub>2</sub>O<sub>3</sub> [11], CeO<sub>2</sub> [12], and SiO<sub>2</sub> [4], have been extensively studied, demonstrating that the catalytic performances

of Au NPs both strongly depend on the intrinsic properties of Au NPs (e.g., particle size [13], shape, distribution, and combinations with other metals), but also relies on the properties of supports (e.g., basicity, acidity, crystal facets, surface functional groups and porous structures). For example, Scott and co-workers synthesized Au nanoclusters and used SiO<sub>2</sub> as a protective shell to encapsulate Au NPs. Under high temperature calcination, Au NPs can still maintain 2–4 nm in size, and have excellent activity for styrene oxidation [14]. Khawaji and co-workers used the sol method to immobilize Au-Pd on different nanostructures CeO<sub>2</sub> and TiO<sub>2</sub> and found that the nanorods CeO<sub>2</sub> and Ti-NTs composite supports are favorable for active metals [15].

One of the effective methods to regulate the catalytic activity, selectivity and stability is to decorate catalyst surfaces by coating inert partial/porous overlayers (e.g., carbonaceous films or silica overlayers) [16,17]. In particular, the inert materials such as stable carbonaceous materials are preferable; for instance, Dai and co-workers employed dopamine as a protective agent and subsequently constructed a carbon shell by high temperature calcination, which promoted the anti-sintering ability of Au NPs and enhanced their electron interaction with support materials [18]. Liu and co-workers reported the phenomenon of electronic perturbation at the Au-carbon interface and its application in controlling the reaction selectivity in styrene oxidation. They confirmed that the N-doped carbon supports generated electron-rich Au surface sites, and the Au-carbon interaction modified the binding behavior of C=C bonds as to catalytic centers [19]. These studies inspired us that biochar could be a potential candidate to serve as the overlayer materials as the biomass and its derivatives are abundant in nature, and the bio-derived compounds and platform chemicals such as lignin, sugar alcohols and aldehydes are already applied in producing catalysts, porous carbon and nanofibers [20,21].

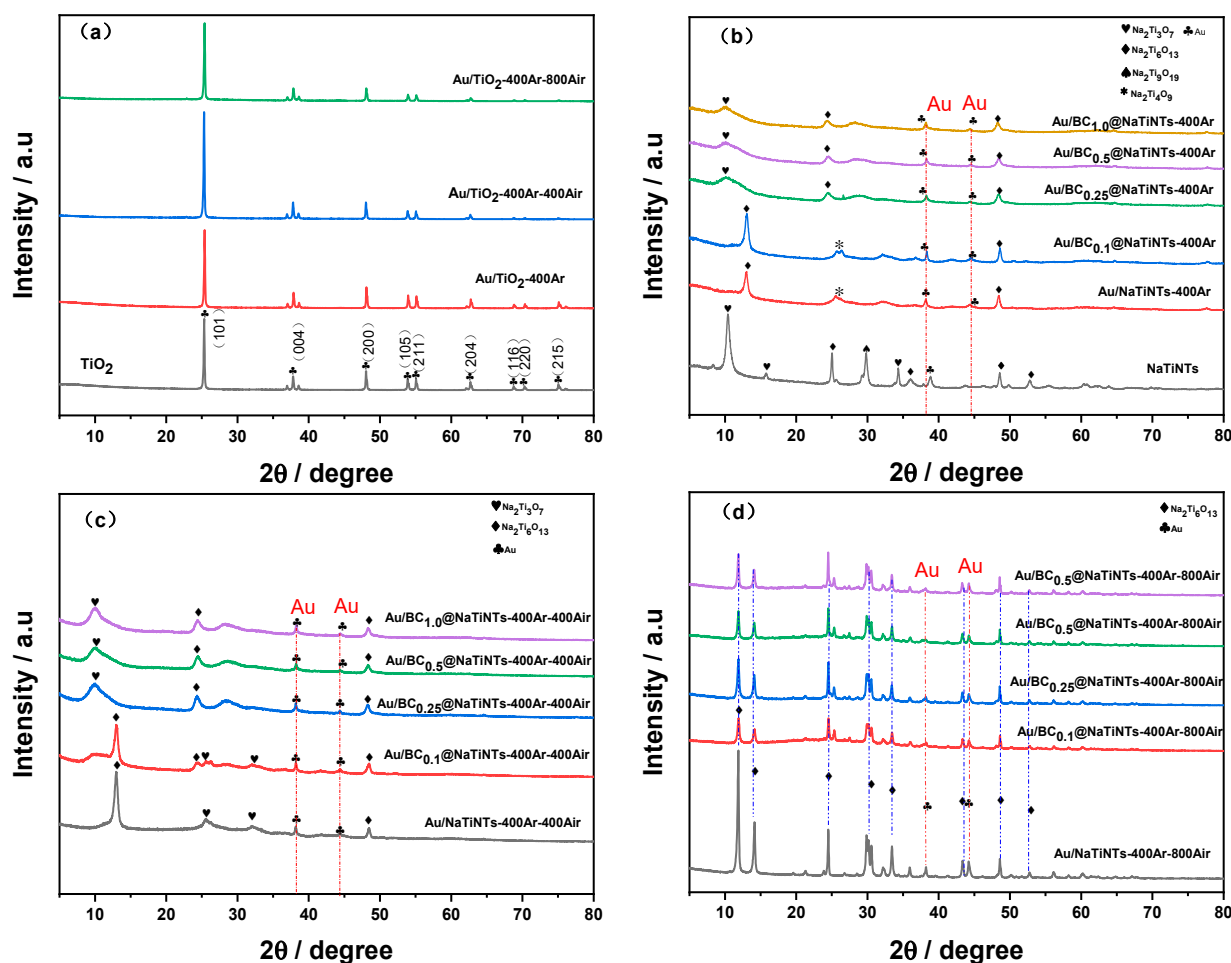
This study aims to explore the dried distiller's grain waste from white wine industries as the biochar source to modify the anatase TiO<sub>2</sub>-derived titanate nanofibers, in order to regulate the catalytic performances of supported Au NPs, and the selective oxidation of benzyl alcohol to benzaldehyde was selected as a model reaction. The choice of distiller's grains could form a hydrochar overlayer on titanate nanofibers under hydrothermal synthetic conditions, and then were transformed into biochar under calcination in the inert gas atmosphere [22]. The catalytic results showed that the change in the content of biochar could effectively improve the selectivity of benzaldehyde, and there existed an optimal content as too high content of biochar inevitably lowered catalytic conversions. Moreover, the influence of reaction time, temperatures, and solvent were also studied using representative catalysts. This paper could provide a strategy to improve catalyst selectivity and stability using biochar to modify catalysts and possibly modify the electronic structure of supported metal catalysts.

## 2. Results and Discussions

### 2.1. Characterizations of Catalysts

#### 2.1.1. Crystal Structures Analysis by XRD

There crystal structures were analyzed by XRD. Figure 1a confirmed that the crystal structures of Au/TiO<sub>2</sub> calcined under different conditions maintained the anatase phase, as compared with commercial TiO<sub>2</sub>. These peaks belonged to the anatase TiO<sub>2</sub> and located at 2θ of 25.3, 36.9, 48.1, 53.9, 55.1, 68.9, 75.1°, which are accordingly attributed to the crystal planes of (101), (004), (200), (105), (211), (116), and (215). However, no diffraction peaks of Au could be observable on the XRD pattern of TiO<sub>2</sub>, and this could be due to several reasons, such as the relatively low real loading of Au as confirmed by ICP (0.64% wt) and the weak peaks of Au that were suppressed by the strong intensity of TiO<sub>2</sub> diffraction peaks [23,24].



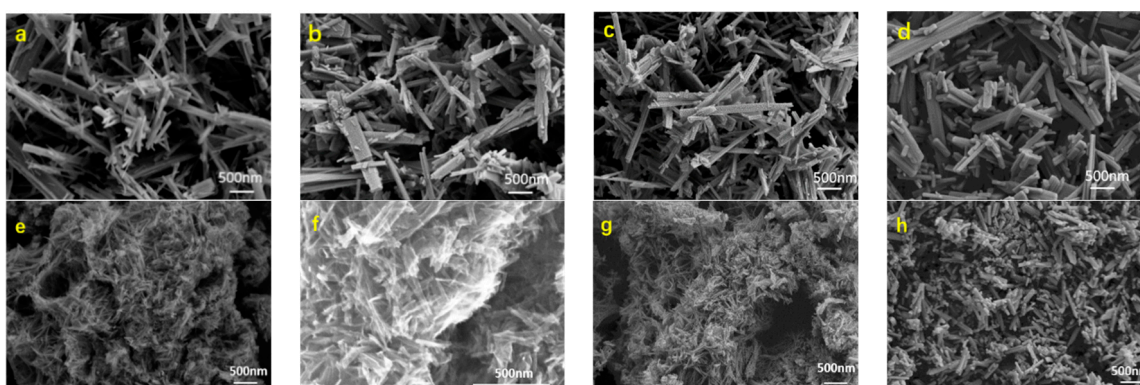
**Figure 1.** XRD patterns of catalyst series calcined at different temperatures: (a) Au/TiO<sub>2</sub>; (b) Au/BC@NaTiNTs-400Ar; (c) Au/BC@NaTiNTs-400Ar-400Air; (d) Au/BC@NaTiNTs-400Ar-800Air.

Figure 1b provided the XRD spectra of Au/BC@NaTiNTs catalysts and compared with that of NaTiNTs which exhibited mainly titanate crystal structures [25] and had a general molecular formula: Na<sub>2</sub>Ti<sub>3</sub>O<sub>7</sub>·nH<sub>2</sub>O (mixed with a trace of Na<sub>2</sub>Ti<sub>4</sub>O<sub>9</sub>, Na<sub>2</sub>Ti<sub>6</sub>O<sub>13</sub>, and Na<sub>2</sub>Ti<sub>9</sub>O<sub>19</sub>). After calcination in Ar at 400 °C, the peak intensities of catalyst support significantly declined. In detail, the peak at 2θ of 10° shifted to 12° as for Au/NaTiNTs-400Ar and Au/BCs<sub>0.10</sub>@NaTiNTs-400Ar, which could be attributed to the loss of intercalated water and the partial conversion of hexatitanate [25]. Interestingly, higher loadings of biochar remained the characteristic peaks at 10° (2θ) and the reasons have not been clarified at current stage. Compared with Au/TiO<sub>2</sub>, the typical peaks of Au can be detected on Au/BC@NaTiNTs-400Ar, indicating that Au NPs are successfully loaded on the carrier.

To partly or completely remove biochar, the Au/BC@NaTiNTs-400Ar catalysts were further calcined in air at different temperatures (400 °C and 800 °C). The XRD spectra of Au/BC@NaTiNTs-400Ar-400Air catalysts were given in Figure 1c, showing that the subsequent calcination in air at 400 °C did not alter the characteristic peaks of the catalysts. When the calcination temperature was raised to 800 °C, the XRD spectra of Au/BC@NaTiNTs-400Ar-800Air were presented in Figure 1d, the peaks of all the catalysts showed similar crystal structures of hexatitanate with a typical sharp peak around 12° (2θ), and the biochar should be completely removed at high temperatures. Characteristic peaks of Au NPs clearly appeared, suggesting that they should be aggregated to relatively larger particles.

### 2.1.2. Morphology Analysis by SEM and TEM

The SEM images in Figure 2 presented two series of catalysts with different calcination pretreatments. The series (a)–(d) were accordingly Au/NaTiNTs, Au/NaTiNTs-400Ar, Au/NaTiNTs-400Ar-400Air, and Au/NaTiNTs-400Ar-800Air, and the series (e)–(h) were biochar-modified Au/BC<sub>0.25</sub>@NaTiNTs, Au/BC<sub>0.25</sub>@NaTiNTs-400Ar, Au/BC<sub>0.25</sub>@NaTiNTs-400Ar-400Air, Au/BC<sub>0.25</sub>@NaTiNTs-400Ar-800Air (the choice of typical loading of 0.25% was based on the catalytic performances and will be discussed later). The SEM images showed that the prepared titanate supports exhibited nanofibrous structures, which facilitated separation from liquid-phase reaction compared with particulate catalysts. As to the catalyst modified by biochar, the nanofibers were thinner, as compared with their counterparts. Nevertheless, the sample of Au/BC<sub>0.25</sub>@NaTiNTs-400Ar-800Air exhibited thicker nanorod-like morphology, compared with that of Au/BC<sub>0.25</sub>@NaTiNTs-400Ar-400Air (more SEM images are provided in Figure S1, ESI).



**Figure 2.** SEM images of (a) Au/NaTiNTs, (b) Au/NaTiNTs-400Ar, (c) Au/NaTiNTs-400Ar-400Air, (d) Au/NaTiNTs-400Ar-800Air, (e) Au/BC<sub>0.25</sub>@NaTiNTs, (f) Au/BC<sub>0.25</sub>@NaTiNTs-400Ar, (g) Au/BC<sub>0.25</sub>@NaTiNTs-400Ar-400Air, (h) Au/BC<sub>0.25</sub>@NaTiNTs-400Ar-800 Air.

### 2.1.3. TEM Analyses and Size Distribution of Au NPs

The morphology of catalysts and the particle size distribution of Au NPs were analyzed by TEM. Figure 3 showed that TEM images and metal particle size distribution histogram of the reference catalysts of Au/TiO<sub>2</sub>-400Ar-400Air and Au/NaTiNTs-400Ar-400Air, and biochar-modified catalysts of Au/BC<sub>0.10</sub>@NaTiNTs-400Ar-400Air, Au/BC<sub>0.25</sub>@NaTiNTs-400Ar-400Air, Au/BC<sub>0.50</sub>@NaTiNTs-400Ar-400Air, Au/BC<sub>1.00</sub>@NaTiNTs-400Ar-400Air (more HR-TEM images were provided in Figure S2, ESI). As can be seen from Figure 3, the Au/NaTiNTs catalysts showed obvious nanofibrous structures, as compared with Au/TiO<sub>2</sub>. For Au/TiO<sub>2</sub> and Au/NaTiNTs catalysts with a relatively low content of biochar, the average particle size of Au NPs was slightly bigger than 7 nm. Nevertheless, the average particle size of Au NPs became smaller on Au/BC<sub>0.50</sub>@NaTiNTs-400Ar-400Air and Au/BC<sub>1.00</sub>@NaTiNTs-400Ar-400Air which had a higher loading of biochar, probably because the surface functional groups (e.g., –OH, –COOH, and =O) hindered that growth of Au NPs during preparation process.

### 2.1.4. Physicochemical Properties of Catalysts

Table 1 summarized the Au content and textural properties of representative catalysts. The nominal loading of Au on all Au/BC@NaTiNTs series catalysts was 1% wt. The ICP results demonstrated that the increase in biochar content gave rise to gradual decline of real Au loading; the real loadings of Au on catalysts are generally lower than the nominal value, owing to the loss of Au during preparation, filtration or washing processes. As shown in Table 1, the surface area of NaTiNTs increased to 21.3 m<sup>2</sup>/g, compared with that of TiO<sub>2</sub> (8.8 m<sup>2</sup>/g). Meanwhile, biochar addition to the NaTiNTs carrier could further increase the specific surface area of the carriers after subsequent carbonization. For

instance, the surface areas reached  $167.5 \text{ m}^2/\text{g}$  for Au/BC<sub>0.25</sub>@NaTiNTs and  $142.9 \text{ m}^2/\text{g}$  for Au/BC<sub>1.00</sub>@NaTiNTs. Interestingly, the surface area of Au/BC<sub>0.50</sub>@NaTiNTs maintained similar to that of TiO<sub>2</sub>, possibly due to the morphological change into nanofibers from nanorods, as shown in Figure 3. This phenomenon was also reported in Hasan and co-worker's work which showed that the surface area of TiO<sub>2</sub> nanofibers was lower than that of nanorods [26]. These results also indicate that the morphology of the carrier can be adjusted by adding different contents of distiller's grains and the intrinsic mechanism on controlling this transformation is worthy of further investigation.

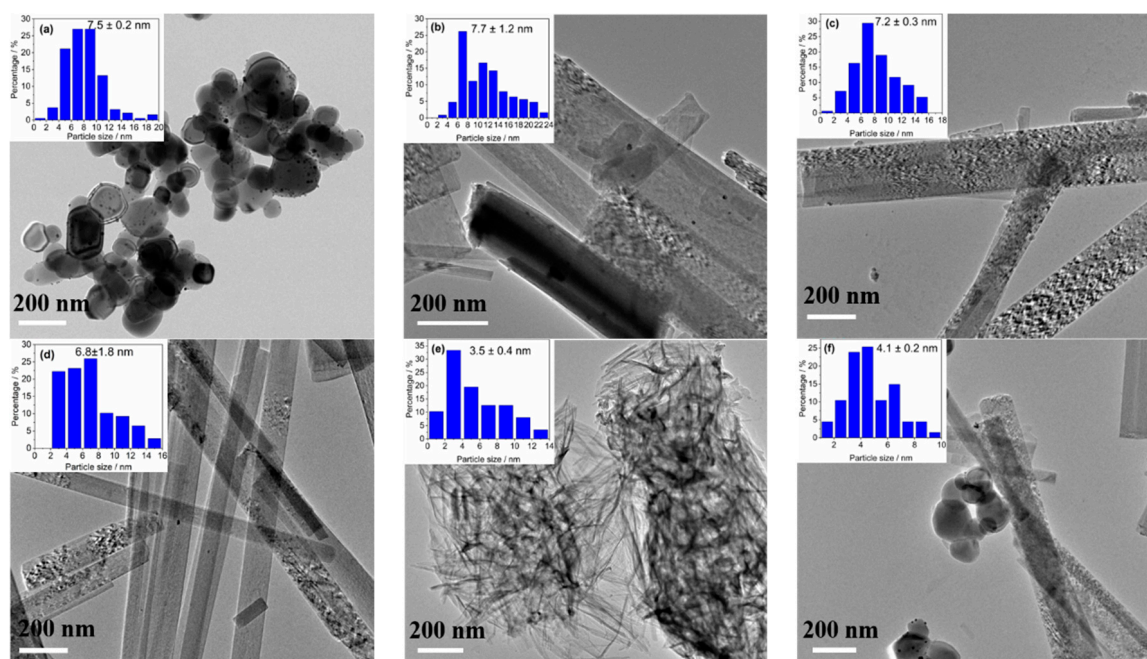


**Figure 3.** TEM images and metal particle size distribution histogram of (a) Au/TiO<sub>2</sub>, (b) Au/NaTiNTs, (c) Au/BC<sub>0.10</sub>@NaTiNTs, (d) Au/BC<sub>0.25</sub>@NaTiNTs, (e) Au/BC<sub>0.50</sub>@NaTiNTs, (f) Au/BC<sub>1.00</sub>@NaTiNTs. **Note:** all the catalysts were calcined at 400 °C in Ar first and then at 400 °C in air.

**Table 1.** The real Au loading and the textural properties of typical catalysts.

Catalyst	Au Loading/%wt	SBET/m <sup>2</sup> g <sup>-1</sup>	Vpore/cm <sup>3</sup> ·g <sup>-1</sup>
Au/TiO <sub>2</sub>	0.64	8.8	0.03
Au/NaTiNTs	1.00	21.3	0.07
Au/BC <sub>0.10</sub> @NaTiNTs	0.90	20.2	0.07
Au/BC <sub>0.25</sub> @NaTiNTs	0.96	167.5	0.65
Au/BC <sub>0.50</sub> @NaTiNTs	0.86	9.2	0.03
Au/BC <sub>1.00</sub> @NaTiNTs	0.56	142.9	0.56

**Note:** all the catalysts were calcined at 400 °C in Ar first and then at 400 °C in air.

### 2.1.5. UV-Vis Characterization of the Catalysts

To confirm the existence of Au NPs on the supports, the UV spectra in the range of 400–800 nm of Au/TiO<sub>2</sub>-400Ar-400Air, Au/NaTiNTs-400Ar-400Air and a series of Au/BC@NaTiNTs-400Ar-400Air catalysts were collected and compared in Figure 4. A strong absorption peak appeared at 200–300 nm (not shown), which originates from the TiO<sub>2</sub> NPs in the material [27]. A wide absorption peak centered around 550 nm and the peaks were characteristic of localized surface plasmon resonance (LSPR), which is generated by the collective oscillation of electrons of Au NPs along with the electromagnetic field of visible light and has been well-studied in literature [28–30], further confirming the well-formed Au NPs on the supports.

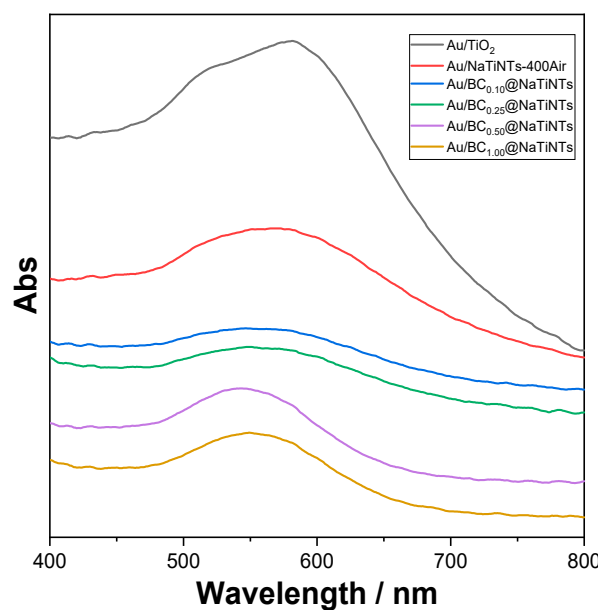


**Figure 4.** UV-vis spectra of Au/TiO<sub>2</sub>, Au/NaTiNTs and series of Au/BC@NaTiNTs. **Note:** all the catalysts were calcined at 400 °C in Ar first and then at 400 °C in air.

#### 2.1.6. XPS Analyses of Key Elements

Figure 5a displayed the high-resolution spectra of Au 4f over the catalyst of Au/NaTiNTs and the series of Au/BC@NaTiNTs catalysts. The XPS spectra of Au can be divided into two peaks, there was a doublet in each XPS spectrum with binding energies (BE) around 83.6 eV and 87.3 eV, corresponding to Au 4f<sub>7/2</sub> and Au 4f<sub>5/2</sub>, respectively. In general, the typical Au 4f<sub>7/2</sub> peak locates at 84.0 eV for bulk metallic Au [31–33], and these results indicated that the Au NPs were mostly in metallic state; nonetheless, with the introduction of the biochar modification, the binding energy slightly shifted from 83.5 eV to about 83.3 eV. According to literature reports, low binding energy indicates that there is a strong electron interaction between Au NPs and the supports, which is beneficial to charge transfer from the supports to Au NPs owing to the strong electronegativity [34–36].

For the elements of C1s, O1s and Ti2p, the high-resolution XPS spectra were also analyzed, offering critical information on the surface species of catalysts. As to the Ti2p shown in Figure 5b, two major spin-orbital peaks of Ti<sup>4+</sup> were observed. The Ti2p<sub>3/2</sub> peak centred at 457.6 eV (Ti<sup>4+</sup>) over four catalysts [37]; however, no peaks of Ti<sup>3+</sup> locating at 454.9 eV were observable [38]. When biochar was introduced to the surface of supports, the slightly negatively-charged Au species was probably due to the electron transfer from carrier to Au [39].

As to other key elements of C1s and O1s, their spectra and detailed analyses by XPS spectra were provided in ESI (Figure S3 and Table S1). The C1s spectra of all catalysts showed the existence of C–C centred at 284.8 eV, C–O centered at 286.5 eV and C=O/O–C=O centred at 288.7 eV [40,41]. The high-resolution XPS spectra of O1s over the four catalysts exhibited four peaks centred around 529.0 eV, 530.6 eV, 532.1 eV and 534.1 eV, and they could be ascribed to the lattice oxygen (Ti–O) or bridging oxygen (Ti=O), oxygen vacancies, the top-site oxygen (–OH/Na or =O) [42], and the surface adsorbed oxygen species [43,44]. According to literature, generation of oxygen vacancies is due to lack of oxygen sites which are supposed to form lattice oxygen sites; hence, the oxygen vacancies tend to adsorb external dissociated oxygen atoms to balance the surface energy and electronic structures [45]; in comparison, the top oxygen species are mainly referred to the surface lattice oxygen with balanced electronic state by connecting cations (e.g., –OH or –ONa) [46].

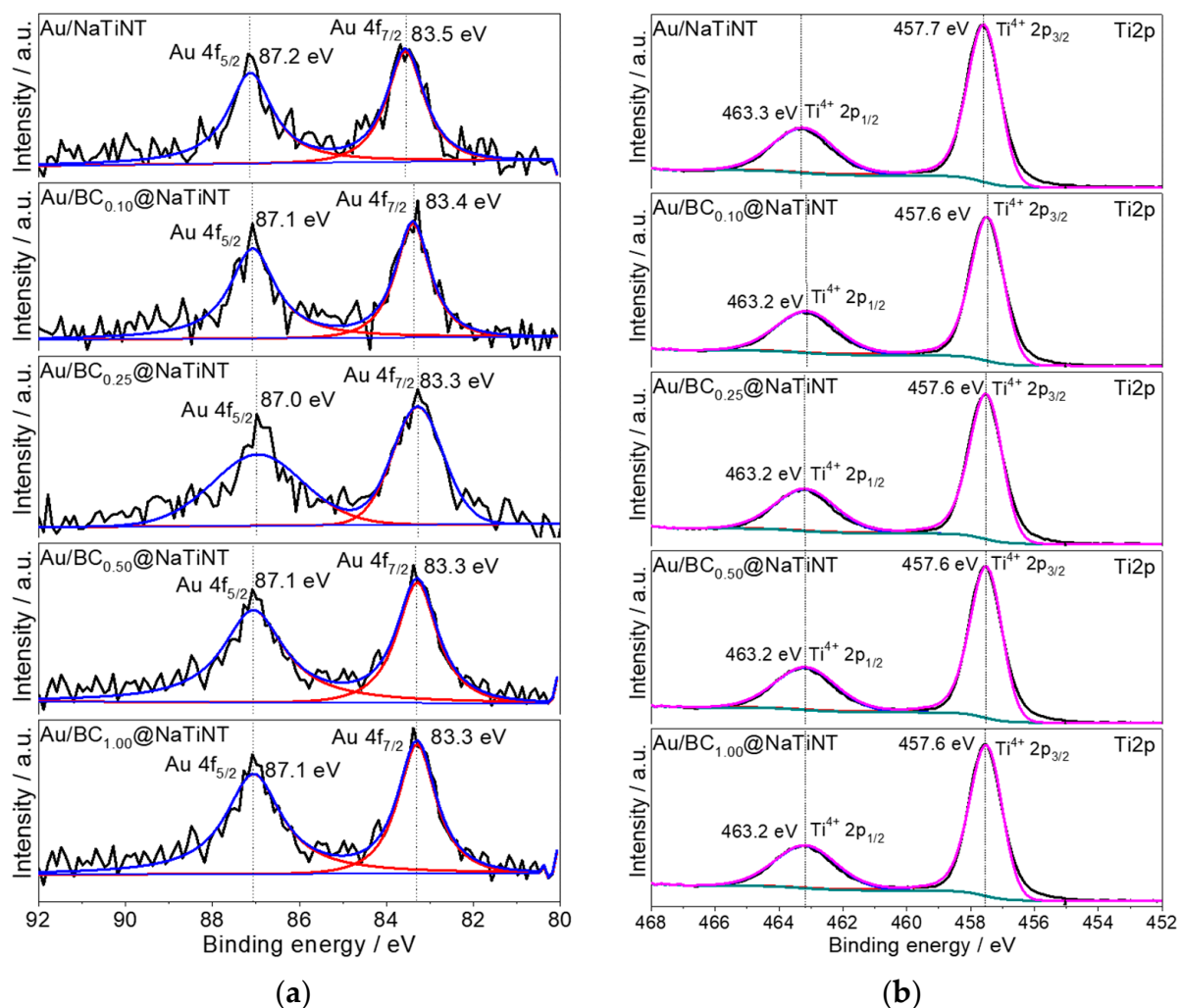


**Figure 5.** XPS spectra of (a) Au 4f of Au/NaTiNTs and a series of Au/BC@NaTiNTs catalysts, (b) Ti 2p of Au/NaTiNTs and series of Au/BC@NaTiNTs. **Note:** all the catalysts were calcined at 400 °C in Ar first and then at 400 °C in air.

## 2.2. Catalytic Performances

### 2.2.1. The Influence of Calcination Temperatures and Biochar Content

The influence of calcination temperatures on catalytic performances was investigated Au/TiO<sub>2</sub>, Au/NaTiNTs, and the series of Au/BC@NaTiNTs catalysts in the selective oxidation of benzyl alcohol to benzaldehyde under atmospheric pressure at 60 °C. All the catalysts were calcined in Ar at 400 °C in the first step to transform hydrochar into biochar, then they were subject to calcination in air at four different temperatures (200, 400, 600, and 800 °C) to partly or completely remove the biochar. As shown in Table 2, the series of Au/TiO<sub>2</sub> catalysts exhibited stable conversion and selectivity, indicating that the calcination in air at different temperatures did not affect their catalytic performances. As for the series of Au/NaTiNTs, the sample calcined at 800 °C in air exhibited a noticeable decline of conversion (10.6%). As to the biochar-modified series of Au/BC@NaTiNTs catalysts, the increase in calcination temperatures did not enhance the catalytic activity for all of them and demonstrated that the calcination in air at 400 °C was an optimal choice in terms of conversion and yield (more information on the reaction rate of benzyl alcohol and the production rate of benzaldehyde was provided in Table S2. They were calculated on the basis of real Au loading detected by ICP).

**Table 2.** The catalytic performances of the selective oxidation of benzyl alcohol over catalysts.

	Calcined in Air	Au/TiO <sub>2</sub>	Au/NaTiNTs	Au/BC <sub>0.10</sub> @NaTiNTs	Au/BC <sub>0.25</sub> @NaTiNTs	Au/BC <sub>0.50</sub> @NaTiNTs	Au/BC <sub>1.00</sub> @NaTiNTs
Con. <sup>a</sup> %	200 °C	30.5	29.9	27.5	11.4	10.0	6.0
	400 °C	31.7	29.3	25.1	24.0	22.8	17.9
	600 °C	27.4	25.9	21.9	23.5	1.9	0.9
	800 °C	34.3	10.6	17.8	24.2	4.3	7.5
Sel. <sup>a</sup> %	200 °C	78.7	51.9	72.5	93.0	99.0	99.0
	400 °C	74.4	58.4	67.0	55.9	92.8	90.5
	600 °C	76.7	66.1	73.1	56.1	99.0	99.0
	800 °C	73.0	69.5	54.3	79.5	99.0	99.0
Yield%	200 °C	24.0	15.5	19.9	10.6	9.9	6.0
	400 °C	23.6	17.1	16.8	13.4	21.2	16.2
	600 °C	21.0	17.1	16.0	13.2	1.8	0.8
	800 °C	25.0	7.4	9.6	19.2	4.3	7.4

<sup>a</sup> Con. refers to conversion; Sel. refers to selectivity. **Reaction conditions:** catalyst (100 mg), benzyl alcohol (4 mmol), toluene (20 mL), NaOH (0.4 mmol), reaction temperature oil bath 60 °C, reaction of 6 h, air atmosphere. **Note:** all the catalysts were calcined at 400 °C in Ar first and then at a certain temperature in air.

The catalytic results of biochar-modified series of Au/BC@NaTiNTs catalysts revealed that the biochar content had a significant influence on the catalytic performances after calcination at a certain temperature (200, 400, 600, and 800 °C). For conversions, the introduction of higher biochar content decreased the conversions over the catalysts of Au/BC@NaTiNTs-400Ar calcined in air at 200, 400, and 800 °C, as compared with the those of the Au/NaTiNTs counterpart. For instance, the conversion (29.3%) on Au/NaTiNTs-400Ar-400Air went down to 17.9% on Au/BC<sub>1.00</sub>@NaTiNTs-400Ar-400Air, while it was 25.9% on Au/NaTiNTs-400Ar-600Air and was almost negligible on Au/BC<sub>1.00</sub>@NaTiNTs-400Ar-600Air. The deactivation of catalysts calcined in air at higher temperatures (600 and 800 °C) was possibly due to the formation of tar transformed from as-produced bio-oil to cover the active sites and the aggregation of Au NPs. On the contrary, calcination in air at 200 °C was unable to remove the biochar obtained by calcination in Ar at 400 °C and the active sites were potentially blocked. Therefore, the optimized calcination temperature was 400 °C in air which retained partial biochar and meanwhile exposed more active sites to ensure catalytic properties, without leading to aggregation of Au NPs. These reasons could explain why Au/BC<sub>0.50</sub>@NaTiNTs-400Ar-400Air exhibited a 22.8% conversion and a 21.2% yield, whereas the conversions and the yields were much lower for calcination in air at 200 °C, 600 °C and 800 °C. For selectivities, a higher biochar content could remarkably increase the selectivity toward benzaldehyde. These results revealed that the catalytic performances could be regulated by biochar modification of supports.

The above results of catalytic performances in Table 2 demonstrated that the optimized calcination temperatures and biochar content, and the series of catalysts calcined at 400 °C in air were selected to explore the influence of reaction time, reaction atmospheres, reaction temperatures and solvent.

### 2.2.2. The Influence of Reaction Time, Atmospheres, and Temperatures

The effect of reaction time (6 h versus 12 h) was given in Figure 6. The conversions remarkably increased as prolongation of reaction time (Figure 6a), while the selectivity maintained at similar level on Au/TiO<sub>2</sub>, Au/NaTiNTs, Au/BC<sub>0.50</sub>@NaTiNTs and Au/BC<sub>1.00</sub>@NaTiNTs and slightly increased on Au/BC<sub>0.10</sub>@NaTiNTs and Au/BC<sub>0.25</sub>@NaTiNTs. These results indicated that the longevity of these catalysts was good under the reaction conditions. Compared with Au/TiO<sub>2</sub> and Au/NaTiNTs, the BC-modified catalysts generally exhibited a higher selectivity, indicating that BC modification has a regulatory effect on the selectivity and is beneficial for improving the selective oxidation of benzyl alcohol to benzaldehyde, while it suppressed further oxidation or other side reactions.

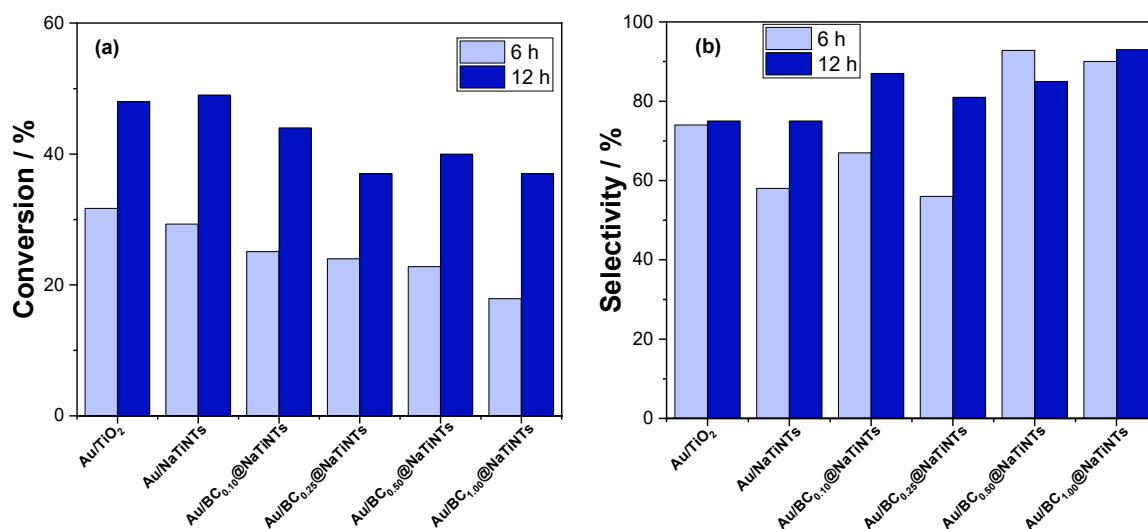


**Figure 6.** The conversion (a) and selectivity (b) of 6 h and 12 h oxidation reaction of air calcined catalyst at 400 °C, **Reaction conditions:** catalyst (100 mg), benzyl alcohol (4 mmol), toluene (20 mL), NaOH (0.4 mmol), reaction temperature oil bath 60 °C, reaction of 6 h, air atmosphere. **Note:** all the catalysts were calcined at 400 °C in Ar first and then at 400 °C in air.

It is well-known that O<sub>2</sub> is a necessary condition for the oxidation of benzyl alcohol; hence, the atmosphere of air and pure O<sub>2</sub> were compared [47], and the results were given in Figure 7. The conversions (Figure 7a) on Au/TiO<sub>2</sub> and Au/NaTiNTs improved and remained similar on the series of Au/BC@NaTiNTs catalysts. As to the selectivity (Figure 7b), all the catalysts showed promoted selectivity toward benzaldehyde to some extent in the atmosphere of O<sub>2</sub>. These results confirmed the benefits of pure O<sub>2</sub> atmosphere.

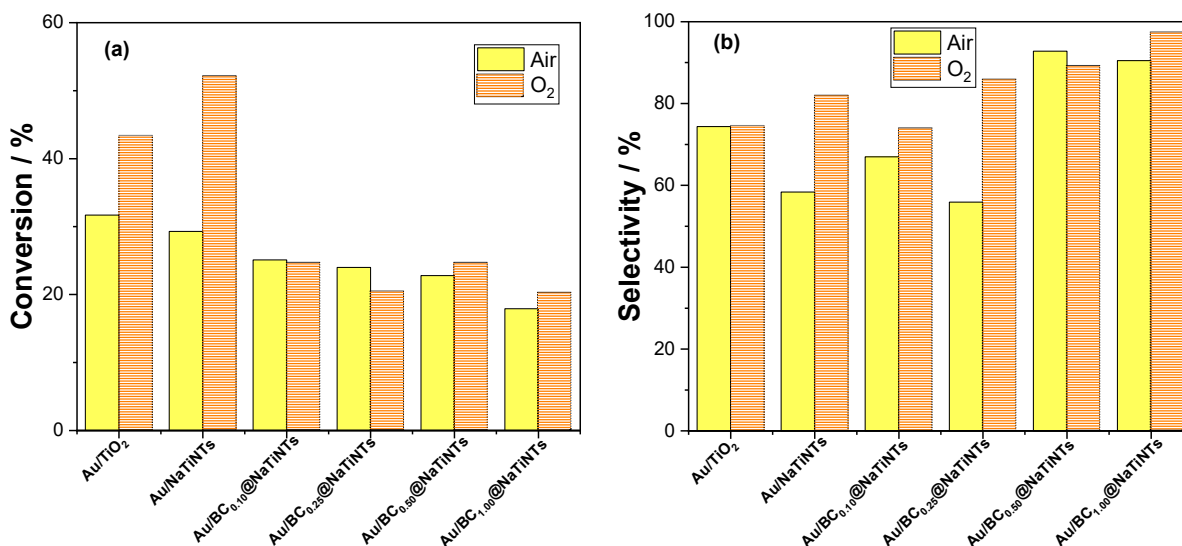


**Figure 7.** The conversion (a) and selectivity (b) of oxidation reaction of 400 °C air calcination catalyst in air and O<sub>2</sub> conditions, **Reaction conditions:** catalyst (100 mg), benzyl alcohol (4 mmol), toluene (20 mL), NaOH (0.4 mmol), reaction temperature oil bath 60 °C, reaction of 6 h, O<sub>2</sub> or air atmosphere. **Note:** all the catalysts were calcined at 400 °C in Ar first and then at 400 °C in air.

Figure 8 compared the catalytic performances of the aforementioned six catalysts at 60 °C and 90 °C with the other conditions being identical. As shown in Figure 8a, all the six catalysts of Au/TiO<sub>2</sub>, Au/NaTiNTs, Au/BC<sub>0.10</sub>@NaTiNTs, Au/BC<sub>0.25</sub>@NaTiNTs, Au/BC<sub>0.50</sub>@NaTiNTs and Au/BC<sub>1.00</sub>@NaTiNTs exhibited enhanced catalytic conversions;

whereas the selectivity (Figure 8b) slightly improved on Au/TiO<sub>2</sub>, Au/NaTiNTs and Au/BC<sub>0.10</sub>@NaTiNTs.

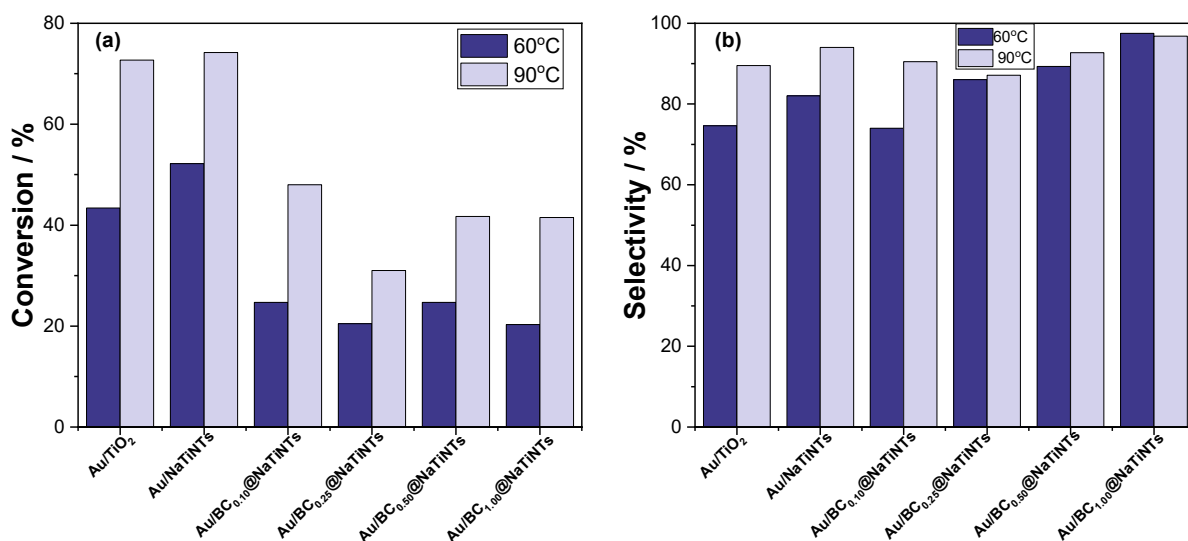


**Figure 8.** The conversion (a) and selectivity (b) of the 400 °C air calcination catalyst at different reaction temperatures, **Reaction conditions:** catalyst (100 mg), benzyl alcohol (4 mmol), toluene (20 mL), NaOH (0.4 mmol), reaction temperature oil bath 60 °C and 90 °C, reaction of 6 h, O<sub>2</sub> atmosphere. **Note:** all the catalysts were calcined at 400 °C in Ar first and then at 400 °C in air.

To sum this part, we investigated the effects of reaction time, gas atmosphere, and temperature on the reactions. All the conversions shown in Figures 6–8 demonstrated that the increase in biochar content lowered the catalytic conversions as compared with those on Au/TiO<sub>2</sub> and Au/NaTiNTs; however, the selectivity toward benzaldehyde generally improved as the biochar content went up, agreeing with the observations in Table 2. Through the test of reaction conditions, the optimal reaction conditions are at 90 °C, 12 h in O<sub>2</sub> atmosphere; nevertheless, we chose to maintain the reaction time at 6 h (12 h meant more energy consumption) through the whole study. These results revealed that adjusting the reaction conditions was able to regulate the catalytic the performance of the catalysts.

### 2.2.3. Reusability Test

The reusability test results of the typical Au/BC<sub>0.10</sub>@NaTiNTs were shown in Figure 9, After each run, the spent catalysts were collected by centrifugation, washed thoroughly with ethanol to remove adsorbed species, and finally were dried overnight at 80 °C. Figure 9 showed that the catalytic selectivity was almost unaffected and the conversions declined very slightly in the five cycles, suggesting decent stability.

To further confirm the key properties of the typical catalysts after five cycles, XRD and TEM characterizations were conducted on the spent Au/BC<sub>0.10</sub>@NaTiNTs catalyst. The TEM images in Figure 10a presented that the morphology of the spent catalyst still maintained the nanorod structures; nonetheless, the results in histogram indicated that a small part of Au NPs aggregated to some extent, as the average diameter of Au NPs increased from 7 nm (fresh catalysts) to about 11 nm. The aggregation of Au NPs could possibly explain the slight decline of catalytic conversions (Figure 9). Figure 10b compared the XRD spectra of the fresh and the spent catalysts, no significant change was observable, except for the slightly intensified diffraction peaks of Au NPs, agreeing with the TEM results.

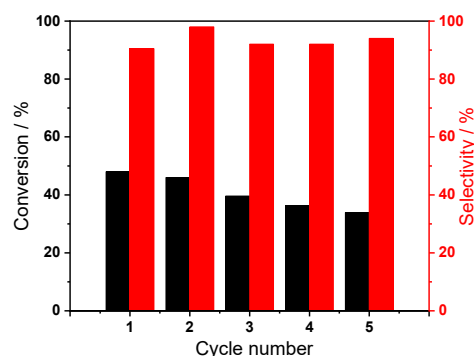


**Figure 9.** Test of reusability Reaction conditions: Au/BC<sub>0.10</sub>@NaTiNTs-400Air (100 mg), benzyl alcohol (4 mmol), toluene (20 mL), NaOH (0.4 mmol), reaction temperature oil bath 90 °C, Reaction of 6 h, O<sub>2</sub> atmosphere. **Note:** For each cycle, the spent catalysts were filtered, washed by ethanol thoroughly to remove intermediates, and fresh catalysts were supplemented to maintain identical catalyst mass.

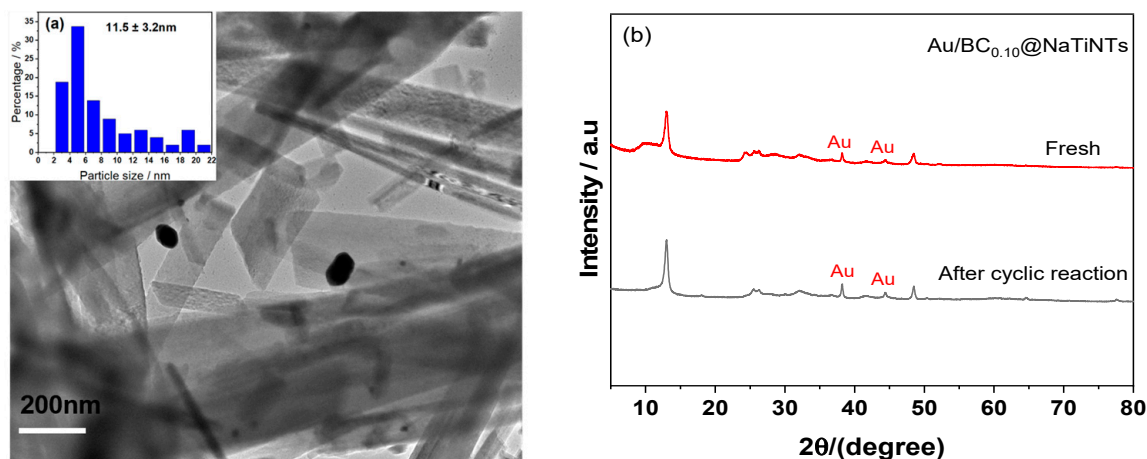


**Figure 10.** (a) TEM images and metal particle size distribution histogram of Au/BC<sub>0.10</sub>@NaTiNTs catalyst after repeatability testing, (b) Comparison of XRD spectra of catalyst Au/BC<sub>0.10</sub>@NaTiNTs before and after reaction.

#### 2.2.4. The Influence of Solvent

For the selective oxidation of benzyl alcohol, the solvent also significantly affects the product distribution. In this study, the solvent of toluene, DMF, hexane, THF and ethanol was examined, using Au/TiO<sub>2</sub>-400Ar-400Air and Au/BC<sub>0.25</sub>@NaTiNTs-400Ar-400Air as the representative catalysts, and the results were examined in Table 3.

**Table 3.** Catalytic results of the selective oxidation of benzyl alcohol in different solvents.

Solvent	Au/TiO <sub>2</sub> -400Ar-400Air			Au/BC <sub>0.25</sub> @NaTiNTs-400Ar-400Air		
	Con. <sup>a</sup> /%	Sel. <sup>a</sup> /%		Con. <sup>a</sup> /%	Sel. <sup>a</sup> /%	
		Benzaldehyde	Others		Benzaldehyde	Others
Toluene	43.4	74.6	– <sup>b</sup>	20.5	86.0	– <sup>b</sup>
DMF	67.9	84.0	Benzene: 16	4.1	99.0	– <sup>c</sup>
Hexane	22.8	57.6	Benzene: 37.9	10.7	99	– <sup>c</sup>
THF	1.9	99	– <sup>c</sup>	2.2	99	– <sup>c</sup>
Ethanol	32.7	5.2	Benzoic acid: 88.8	<1	– <sup>b</sup>	– <sup>b</sup>

<sup>a</sup> Con. refers to conversion; Sel. refers to selectivity. <sup>b</sup> No other quantifiable products were detected. <sup>c</sup> The content of products was too low to be quantifiable. **Reaction conditions:** catalyst (100 mg), benzyl alcohol (4 mmol), solvent (20 mL), NaOH (0.4 mmol), reaction temperature oil bath 60 °C, reaction of 6 h, O<sub>2</sub> atmosphere.

Except for ethanol, the main product was benzaldehyde in the other four catalysts. In toluene, no other products were detected, though the selectivity was 74.6% over Au/TiO<sub>2</sub>-400Ar-400Air and 86.0% Au/BC<sub>0.25</sub>@NaTiNTs-400Ar-400Air, possibly overlapped by the peak of toluene, as some studies reported that toluene was a potential by-product [48]. In DMF and hexane, another quantifiable product was benzene over Au/TiO<sub>2</sub>-400Ar-400Air, and possible by-products such as benzoic acid, toluene, ethers and esters were unquantifiable [49]; In comparison, the selectivity toward benzaldehyde was excellent over the Au/BC<sub>0.25</sub>@NaTiNTs-400Ar-400Air, owing the biochar modification. Yegzhu and co-workers research also showed that DMF as solvent was beneficial to the formation of aldehyde in benzyl alcohol oxidation reaction [50]. The activity of catalysts in THF solvent was very low, which was similar to the reported results in Mao and co-workers' study and the plausible reason could be due to competitive adsorption between solvent molecules and reactant molecules. The solvent molecules with higher polarity were easier to be adsorbed on the catalysts to occupy or reduce the accessibility of active sites, which hindered the activation of reactant molecules and thus reduced the catalytic conversions [51]. From another point of view, Duarte and co-workers investigate the effect of solvent properties on the benzyl alcohol oxidation reaction [52], proposing that high oxygen solubility in nonpolar solvents favors oxidation.

Other factors were also considered, such as the relationship between the alkalinity of the solvent and the reaction rate, and the moderate hydrogen bond accommodation ability of the solvent, as these factors can affect the interaction between the solvent and benzyl alcohol. Admittedly, the intrinsic mechanism of solvent effect was still unclear, including the effect of solvent polarity, solvent ability to dissolve oxygen, and the adsorption/desorption of the intermediate products [53,54]. For example, the primary product was benzoic acid over Au/TiO<sub>2</sub>-400Ar-400Air in ethanol, whereas the reaction was almost stopped over Au/BC<sub>0.25</sub>@NaTiNTs-400Ar-400Air in ethanol, indicating that the biochar modification of supports strongly affected the catalytic mechanism.

### 3. Experimental Parts

#### 3.1. Raw Materials

The original wet distillers' grains with solubles were provided from Moutai Institute, Renhuai city of Guizhou Province, China. The samples were dried in an oven at 105 °C for 8 h. The dried distiller's grains (DDGs) were pulverized into particles by swing multifunction pulverizer with particle sizes being smaller than 0.3 mm (by 50 mesh screen), and were stored in a desiccator at room temperature. Raw materials and chemicals such as TiO<sub>2</sub> (99%, 325 mesh, anatase powders), gold (III) chloride trihydrate (HAuCl<sub>4</sub>·3H<sub>2</sub>O, Au content: 48–50%), L-lysine (98%), sodium borohydride (NaBH<sub>4</sub>, 98%), sodium hydroxide (NaOH, 96%), benzyl alcohol (99%), benzaldehyde (99%), toluene (99.8%), N, N-dimethylformamide (DMF, 99.5%), tetrahydrofuran (THF, 99.9%), ethanol (99.5%) and hexane (98%) were purchased from Aladdin Industrial Inc. (Shanghai, China).

#### 3.2. Catalyst Preparation

**Support precursors:** The support precursors of DDGs-derived hydrochar-coated titanate nanofibers were prepared first. The preparation method was according to the reference [55]. Typically, 1 g of TiO<sub>2</sub> were mixed in 15 mL of 10 mol/L NaOH first in a glass beaker and were stirred using a magnetic bar at room temperature for 2 h to disperse powders, followed by ultrasonication for 0.5 h. Five identical samples were prepared at the same time, 0.1 g, 0.25 g, 0.5 g and 1.00 g of DDGs powders were added, respectively, further mixing for 20 h under stirring. The five samples were transferred into five autoclaves (50 mL) and placed in an oven and maintained at 180 °C for 48 h under static conditions. The obtained solid products were fully washed with distilled water until the pH of filtrate reached 7–9 and finally were washed by ethanol. The products were dried at 80 °C overnight.

**Loading of Au NPs.** Au NPs were immobilized on the support precursors by a chemical reduction method according to our previous report [48]. Briefly, 1 g of the above-mentioned support precursors (hydrochar-modified titanate nanofibers) were dispersed in 50 mL of deionized water. The suspension was stirred at room temperature for 10 min and then sonicated in an ultrasonic bath for 10 min. To the above suspension, 10 mL of  $5.08 \times 10^{-3}$  mol/L H<sub>2</sub>AuCl<sub>4</sub> solution was added to obtain a theoretical loading of Au (1% wt). Under vigorous stirring for 10 min, 10 mL of 0.53 mol/L lysine solution was added dropwise to the suspension and the stirring was prolonged for 30 min. After this, 10 mL of 0.35 mol/L NaBH<sub>4</sub> solution was added dropwise to reduce H<sub>2</sub>AuCl<sub>4</sub>, and the mixture was stirred for 1 h. After stirring, the suspension was aged for 24 h. The obtained solid was washed with deionized water until the pH of filtrate reached 7–8 and then the products were washed once with 10 mL of ethanol for each sample.

**Calcination treatment.** Above all, the catalysts were calcined in a tube furnace at 400 °C in Ar flow (40 mL/min) for 2 h to transform the surface hydrochar into biochar. The obtained catalysts were denoted as Au/NaTiNTs-400Ar, Au/BC<sub>0.10</sub>NaTiNTs-400Ar, Au/BC<sub>0.25</sub>NaTiNTs-400Ar, Au/BC<sub>0.50</sub>NaTiNTs-400Ar and Au/BC<sub>1.00</sub>NaTiNTs-400Ar. To further confirm the influence of biochar content, the above samples were calcined in air in a muffle furnace at different temperatures (200 °C–800 °C) to partially or completely remove biochar, and the sample was denoted as the following, for instance, Au/BC<sub>0.25</sub>NaTiNTs-400Ar-400Air, meaning that the catalyst of Au/BC<sub>0.25</sub>NaTiNTs-400Ar was further calcined in air at 400 °C. The reference catalyst of Au/TiO<sub>2</sub> was also calcined using the same procedure for comparison.

**Synthesis of control catalysts of Au/HTiNTs and Au/TiO<sub>2</sub>.** The preparation method of the titanate support was the same as the above-mentioned synthesis of Na-form titanate nanofibers (NaTiNTs). Then, NaTiNTs were ion-exchange with HCl solution to give H-form titanate nanofibers (HTiNTs). Au NPs were immobilized on HTiNTs or TiO<sub>2</sub> (anatase) supports using the same chemical reduction method [56,57].

### 3.3. Catalyst Characterization

The supports and catalyst samples were analyzed using a Rigaku Smartlab diffractometer and Cu K $\alpha$  radiation, and the crystallinity and phase of the samples were determined by powder X-ray diffraction (XRD) at a scan rate of  $2\theta = 5\sim 80^\circ$  at  $5^\circ$  min and a voltage of 40 kV. They were analyzed by scanning electron microscope (SEM) with Zeiss Gemini 300, and the voltage was 25 kV. The real Au loading on catalysts was analyzed on an Agilent 5110 Inductively Coupled Plasma Atomic Emission Spectrometer (ICP-OES). UV-vis absorbance spectra were acquired on Shimadzu UV-2600 PC spectrophotometer with an ISR-240A integrating sphere attachment to examine their optical properties. X-ray photoelectron spectroscopy (XPS) was conducted on a Kratos Axis HSi X-ray photoelectron spectrometer fitted with a charge neutralizer and magnetic focusing lens, utilizing Al K $\alpha$  monochromatic radiation (1486.7 eV). The morphologies of catalysts and the size distribution of Au NPs were also examined by transmission electron microscopy (TEM) over a JEOL JEM-200 apparatus with an operating voltage of 200 kV. The Brunner-Emmett-Teller (BET) specific surface area was measured by a Micromeritics ASAP 2460 device using adsorption and desorption of N<sub>2</sub> at the temperature of 77 K.

### 3.4. Catalytic Tests

The prepared series of catalysts were evaluated in the selective oxidation of benzyl alcohol, and test conditions were on the basis our previous study [48]. The reactor was a 100 mL round-bottomed Pyrex glass flask sealed with a rubber spigot. An oil bath was used to control the reaction temperature. The reactant of benzyl alcohol (4 mmol) was dissolved into the solvent of toluene (20 mL). The base NaOH (0.4 mmol, molar ratio 0.4/4 = 10% as to reactant) and the catalysts (100 mg) were added into the mixture (the mass transfer was ruled out under these conditions). Bases were reported to act as initiators or promoters to enhance the de-protonation of alcohol molecules by initializing activation of C–H and

O–H on alcohols, thus reducing energy barriers to form intermediates or products [58,59]. The reaction solution with catalysts was stirred for 2 h at room temperature to rule out the adsorption effect, and the change in benzyl alcohol content was quantified by GC [60]. The results showed that the change in the concentration of benzyl alcohol could not be quantifiable, excluding the adsorption of benzyl alcohol on the catalysts and its contribution to conversions. For benzaldehyde, similar tests were performed and no quantifiable change in benzaldehyde concentration was detected after the adsorption tests. For sampling, a plastic syringe with a Millipore nylon filter (pore size 0.22  $\mu\text{m}$ ) was used. 1 mL of aliquots were filtered to saturate the filter, then another 1 mL of reaction solution was taken using the same filter.

To identify and quantify reactants and products [61], the samples were analyzed on a Gas Chromatograph (GC 9720P, produced by Zhejiang FULLI, Hangzhou, China) equipped with the HP-5 column (Agilent J&W GC Columns, Santa Clara, CA, USA, HP-5, length 30 m, diameter 0.320 mm, film thickness 0.25 microns). In detail, each standard sample, such as benzyl alcohol and benzaldehyde, was conducted in triplicate with a peak area reproducibility of  $\pm 2\%$  for standards and  $\pm 10\%$  for samples with low-concentration product. Response factors were determined from respective multipoint calibration curves. The conversion of benzyl alcohol and product selectivity were calculated according to the following equations:

$$\text{Conversion (\%)} = \frac{\text{moles of reactant}_{t=0} - \text{moles of reactant}_{t=6}}{\text{moles of reactant}_{t=0}} \times 100$$

$$\text{Selectivity (\%)} = \frac{\text{moles of product}_{t=6}}{\text{moles of reactant}_{t=0} - \text{moles of reactant}_{t=6}} \times 100$$

#### 4. Conclusions

In summary, a series of Au/BC@NaTiNTs catalysts were developed and tested in the selective oxidation of benzyl alcohol. The test results proved that the introduction of biochar on the catalyst supports declined catalytic conversions, whereas the selectivity toward target product of benzaldehyde was improved. After calcination in air at different temperatures to partly or completely remove the biochar also affected the catalytic performances, in particular, the catalytic conversions decreased if the catalysts were subject to high-temperature calcination (600–800  $^{\circ}\text{C}$ ), possibly owing to the aggregation or the coverage of Au NPs, and 400  $^{\circ}\text{C}$  was the optimal calcination temperature. The tests of reaction conditions such as temperatures, time, atmospheres and solvent demonstrated their effects on the catalytic activity and selectivity and could help to optimize the catalytic performances, combining with biochar modification.

**Supplementary Materials:** The following supporting information can be downloaded at: <https://www.mdpi.com/article/10.3390/catal13050864/s1>, SEM images, TEM images, XPS analysis and Comparison of reaction rates based on ICP tests.

**Author Contributions:** The work was proposed and supervised by X.Z. X.C. conducted most of the experimental parts and data analyses, H.J. and D.C. conducted parts of experiments and helped data collection. The manuscript was written by X.Z. and revised by K.L. and X.K. S.Y. and J.C. co-supervised the project. All authors have read and agreed to the published version of the manuscript.

**Funding:** The authors thank the program for Professor of Special Appointment (Eastern Scholar) at Shanghai Institutions of Higher Learning in 2019. Junmeng Cai specially thanks the financial support from Sino-German Center for Research Promotion (Project No.: M-0183). Shirui Yu specially thanks the Scientific and Technological Support Project ([2019]2370) and the Special Funds for Local Scientific and Technological Development Guided by the Central Government ([2019]4006) from Guizhou Science and Technology Department for financial supports.

**Data Availability Statement:** Data are contained within the article or supplementary material.

**Conflicts of Interest:** The authors declare no conflict of interest.

## References

1. Yadav, G.D.; Mewada, R.K.; Manyar, H.; Wagh, D.P. Advances and future trends in selective oxidation catalysis: A critical review. *Catal. Sci. Technol.* **2022**, *12*, 7245–7269. [[CrossRef](#)]
2. Xiao, Y.H.; Liang, L.; Liu, Z.Z.; Yin, X.; Yang, X.J.; Ding, Y.G.; Du, Z.P. Facile fabrication of size-controlled Pd nanoclusters supported on Al<sub>2</sub>O<sub>3</sub> as excellent catalyst for solvent-free aerobic oxidation of benzyl alcohol. *Appl. Surf. Sci.* **2022**, *585*, 152668. [[CrossRef](#)]
3. Li, Y.Y.; Sabbaghi, A.; Huang, J.; Li, K.C.; Tsui, L.S.; Lam, F.L.Y.; Hu, X.J. Aerobic oxidation of benzyl alcohol: Influence from catalysts basicity, acidity, and preparation methods. *Mol. Catal.* **2020**, *485*, 110789. [[CrossRef](#)]
4. Lv, X.S.; Yuan, S.H.; Zhang, Y.W.; Fu, Y.F.; Wu, Y.J.; Zhou, Y.M.; Huang, R.; Huang, Z.W. Preparation of cyclonic Co<sub>3</sub>O<sub>4</sub>/Au/mesoporous SiO<sub>2</sub> catalysts with core-shell structure for solvent-free oxidation of benzyl alcohol. *J. Taiwan. Inst. Chem. Eng.* **2019**, *102*, 448–455. [[CrossRef](#)]
5. Villa, A.; Dimitratos, N.; Chan, T.C.E.; Hammond, C.; Veith, G.M.; Wang, D.; Manzoli, M.; Prati, L.; Hutchings, G.J. Characterisation of gold catalysts. *Chem. Soc. Rev.* **2016**, *45*, 4953–4994. [[CrossRef](#)]
6. Xu, Y.; Li, J.; Zhou, J.; Liu, Y.F.; Wei, Z.J.; Zhang, H. Layered double hydroxides supported atomically precise Au nanoclusters for air oxidation of benzyl alcohol: Effects of size and active site structure. *J. Catal.* **2020**, *389*, 409–420. [[CrossRef](#)]
7. Sankar, M.; He, Q.; Engel, R.V.; Sainna, M.A.; Logsdail, A.J.; Roldan, A.; Willock, D.J.; Agarwal, N.; Kiely, C.J.; Hutchings, G.J. Role of the support in gold-containing nanoparticles as heterogeneous catalysts. *Chem. Rev.* **2020**, *120*, 3890–3938. [[CrossRef](#)]
8. Brindle, J.; Sufyan, S.A.; Nigra, M.M. Support, composition, and ligand effects in partial oxidation of benzyl alcohol using gold-copper clusters. *Catal. Sci. Technol.* **2022**, *12*, 3846–3855. [[CrossRef](#)]
9. Hao, Y.; Wang, S.; Sun, Q.; Shi, L.; Lu, A.H. Uniformly dispersed Pd nanoparticles on nitrogen-doped carbon nanospheres for aerobic benzyl alcohol oxidation. *Chin. J. Catal.* **2015**, *36*, 612–619. [[CrossRef](#)]
10. Li, X.L.; Feng, J.J.; Sun, J.; Wang, Z.; Zhao, W. Solvent-free catalytic oxidation of benzyl alcohol over Au-Pd bimetal deposited on TiO<sub>2</sub>: Comparison of rutile, brookite, and anatase. *Nanoscale Res. Lett.* **2019**, *14*, 394. [[CrossRef](#)]
11. Ndolomingo, M.J.; Meijboom, R. Selective liquid phase oxidation of benzyl alcohol to benzaldehyde by tert-butyl hydroperoxide over  $\gamma$ -Al<sub>2</sub>O<sub>3</sub> supported copper and gold nanoparticles. *Appl. Surf. Sci.* **2017**, *398*, 19–32. [[CrossRef](#)]
12. Zhou, Q.Y.; Zhou, C.Y.; Zhou, Y.H.; Hong, W.; Zou, S.H.; Gong, X.Q.; Liu, J.J.; Xiao, L.p.; Fan, J. More than oxygen vacancies: A collective crystal-plane effect of CeO<sub>2</sub> in gas-phase selective oxidation of benzyl alcohol. *Catal. Sci. Technol.* **2019**, *9*, 2960–2967. [[CrossRef](#)]
13. Ishida, T.; Murayama, T.; Taketoshi, A.; Haruta, M. Importance of size and contact structure of gold nanoparticles for the genesis of unique catalytic processes. *Chem. Rev.* **2019**, *120*, 464–525. [[CrossRef](#)] [[PubMed](#)]
14. Sudheeshkumar, V.; Shivhare, A.; Scott, R.W.J. Synthesis of sinter-resistant Au@silica catalysts derived from Au<sup>25</sup> clusters. *Catal. Sci. Technol.* **2016**, *7*, 272–280. [[CrossRef](#)]
15. Khawaji, M.; Chadwick, D. Au–Pd NPs immobilised on nanostructured ceria and titania: Impact of support morphology on the catalytic activity for selective oxidation. *Catal. Sci. Technol.* **2018**, *8*, 2529–2539. [[CrossRef](#)]
16. Zaarour, M.; Cazemier, J.; Ruiz-Martínez, J. Recent developments in the control of selectivity in hydrogenation reactions by confined metal functionalities. *Catal. Sci. Technol.* **2020**, *10*, 8140–8172. [[CrossRef](#)]
17. Otor, H.O.; Steiner, J.B.; García-Sancho, C.; Alba-Rubio, A.C. Encapsulation methods for control of catalyst deactivation: A Review. *ACS Catal.* **2020**, *10*, 7630–7656. [[CrossRef](#)]
18. Zhan, W.; He, Q.; Liu, X.; Guo, Y.; Wang, Y.; Wang, L.; Guo, Y.; Borisevich, A.Y.; Zhang, J.; Lu, G.; et al. A sacrificial coating strategy toward enhancement of metal-support interaction for ultrastable Au nanocatalysts. *J. Am. Chem. Soc.* **2016**, *138*, 16130–16139. [[CrossRef](#)]
19. Liu, B.; Wang, P.; Lopes, A.; Jin, L.; Zhong, W.; Pei, Y.; Suib, S.L.; He, J. Au-carbon electronic interaction mediated selective oxidation of styrene. *ACS Catal.* **2017**, *7*, 3483–3488. [[CrossRef](#)]
20. Do Minh, T.; Song, J.; Deb, A.; Cha, L.; Srivastava, V.; Sillanpää, M. Biochar based catalysts for the abatement of emerging pollutants: A review. *Chem. Eng. J.* **2020**, *394*, 124856. [[CrossRef](#)]
21. Szcześniak, B.; Phuriragpitikhon, J.; Choma, J.; Jaroniec, M. Recent advances in the development and applications of biomass-derived carbons with uniform porosity. *J. Mater. Chem. A* **2020**, *8*, 18464–18491. [[CrossRef](#)]
22. Dong, X.S.; Wang, Y.Q.; Jia, M.M.; Niu, Z.Y.; Cai, J.M.; Yu, X.; Ke, X.B.; Yao, J.F.; Zhang, X.G. Sustainable and scalable in-situ synthesis of hydrochar-wrapped Ti<sub>3</sub>AlC<sub>2</sub>-derived nanofibers as adsorbents to remove heavy metals. *Bioresour. Technol.* **2019**, *282*, 222–227. [[CrossRef](#)] [[PubMed](#)]
23. Cojocar, B.; Andrei, V.; Tudorache, M.; Lin, F.; Cadigan, C.; Richards, R.; Parvulescu, V.I. Enhanced photo-degradation of bisphenol pollutants onto gold-modified photocatalysts. *Catal. Today* **2016**, *284*, 153–159. [[CrossRef](#)]
24. Gregor, Ž.; Matevž, R.; Janez, Z.; Janez, K.; Albin, P. Effect of Au loading on Schottky barrier height in TiO<sub>2</sub> + Au plasmonic photocatalysts. *Appl. Surf. Sci.* **2021**, *579*, 152196.
25. Lu, Y.M.; Zhu, H.Z.; Liu, J.W.; Yu, S.H. Palladium nanoparticles supported on titanate nanobelts for solvent-free aerobic oxidation of alcohols. *ChemCatChem* **2015**, *7*, 4131–4136. [[CrossRef](#)]

26. Jamal, H.; Kang, B.S.; Lee, H.; Yu, J.S.; Lee, C.S. Comparative Studies of Electrochemical Performance and Characterization of TiO<sub>2</sub>/Graphene Nanocomposites as Anode Materials for Li-Secondary Batteries. *J. Ind. Eng. Chem.* **2018**, *64*, 151–166. [[CrossRef](#)]
27. Song, K.; Wang, X.H.; Xiang, Q.; Xu, J.Q. Weakened negative effect of Au/TiO<sub>2</sub> photocatalytic activity by CdS quantum dots deposited under UV-vis light illumination at different intensity ratios. *Phys. Chem. Chem. Phys.* **2016**, *18*, 29131–29138. [[CrossRef](#)]
28. Corro, G.; Cebada, S.; Pal, U.; Fierro, J.L.G. Au<sup>0</sup>–Au<sup>3+</sup> bifunctional site mediated enhanced catalytic activity of Au/ZnO composite in diesel particulate matter oxidation. *J. Catal.* **2017**, *347*, 148–156. [[CrossRef](#)]
29. Hernández Ramírez, E.; Wang, J.A.; Chen, L.F.; Valenzuela, M.A.; Dalai, A.K. Partial oxidation of methanol catalyzed with Au/TiO<sub>2</sub>, Au/ZrO<sub>2</sub> and Au/ZrO<sub>2</sub>-TiO<sub>2</sub> catalysts. *Appl. Surf. Sci.* **2017**, *399*, 77–85. [[CrossRef](#)]
30. Pan, Y.N.; Wu, G.D.; He, Y.F.; Feng, J.T.; Li, D.Q. Identification of the Au/ZnO interface as the specific active site for the selective oxidation of the secondary alcohol group in glycerol. *J. Catal.* **2018**, *369*, 222–232. [[CrossRef](#)]
31. Wong, R.J.; Scott, J.; Kappen, P.; Low, G.K.C.; Hart, J.N.; Amal, R. Enhancing bimetallic synergy with light: The effect of UV light pre-treatment on catalytic oxygen activation by bimetallic Au–Pt nanoparticles on a TiO<sub>2</sub> support. *Catal. Sci. Technol.* **2017**, *7*, 4792–4805. [[CrossRef](#)]
32. Yu, Y.; Wen, W.; Qian, X.Y.; Liu, J.B.; Wu, J.M. UV and visible light photocatalytic activity of Au/TiO<sub>2</sub> nanoforests with anatase/rutile phase junctions and controlled Au locations. *Sci. Rep.* **2017**, *7*, 41253. [[CrossRef](#)] [[PubMed](#)]
33. Deas, R.; Pearce, S.; Goss, K.; Wang, Q.; Chen, W.T.; Waterhouse, G.I.N. Hierarchical Au/TiO<sub>2</sub> nanoflower photocatalysts with outstanding performance for alcohol photoreforming under UV irradiation. *Appl. Catal. A Gen.* **2020**, *602*, 117706. [[CrossRef](#)]
34. Khawaji, M.; Chadwick, D. Au-Pd bimetallic nanoparticles immobilised on titanate nanotubes: A highly active catalyst for selective oxidation. *ChemCatChem* **2017**, *9*, 4353–4363. [[CrossRef](#)]
35. Khawaji, M.; Chadwick, D. Selective oxidation using Au-Pd catalysts: Role of the support in the stabilization of colloidal Au-Pd NPs. *Catal. Today* **2019**, *348*, 203–211. [[CrossRef](#)]
36. Chen, D.; Shi, J.; Shen, H.Y. High-dispersed catalysts of core-shell structured Au@SiO<sub>2</sub> for formaldehyde catalytic oxidation. *Chem. Eng. J.* **2019**, *385*, 123887. [[CrossRef](#)]
37. Aramendía, M.A.; Borau, V.; Colmenares, J.C.; Marinas, A.; Marinas, J.M.; Navío, J.A.; Urbano, F.J. Modification of the photocatalytic activity of Pd/TiO<sub>2</sub> and Zn/TiO<sub>2</sub> systems through different oxidative and reductive calcination treatments. *Appl. Catal. B Environ.* **2008**, *80*, 88–97. [[CrossRef](#)]
38. Soundiraraju, B.; George, B.K. Two-dimensional titanium nitride (Ti<sub>2</sub>N) MXene: Synthesis, characterization, and potential application as surface-enhanced raman scattering substrate. *ACS Nano* **2017**, *11*, 8892–8900. [[CrossRef](#)]
39. Wu, Y.M.; Zhang, J.L.; Xiao, L.; Chen, F. Preparation and characterization of TiO<sub>2</sub> photocatalysts by Fe<sup>3+</sup> doping together with Au deposition for the degradation of organic pollutants. *Appl. Catal. B Environ.* **2008**, *88*, 525–532. [[CrossRef](#)]
40. Peng, C.; Yang, X.F.; Li, Y.H.; Yu, H.; Wang, H.J.; Peng, F. Hybrids of two-dimensional Ti<sub>3</sub>C<sub>2</sub> and TiO<sub>2</sub> exposing {001} facets toward enhanced photocatalytic activity. *ACS Appl. Mater. Interfaces* **2016**, *8*, 6051–6060. [[CrossRef](#)]
41. Li, D.F.; Wang, J.G.; Xu, F.X.; Zhang, N.C.; Men, Y. Mesoporous (001)-TiO<sub>2</sub> nanocrystals with tailored Ti<sup>3+</sup> and surface oxygen vacancies for boosting photocatalytic selective conversion of aromatic alcohols. *Catal. Sci. Technol.* **2021**, *11*, 2939–2947. [[CrossRef](#)]
42. Wang, K.; Lu, J.B.; Lu, Y.; Lau, C.H.; Zheng, Y.; Fan, X.F. Unravelling the CC coupling in CO<sub>2</sub> photocatalytic reduction with H<sub>2</sub>O on Au/TiO<sub>2</sub>-x: Combination of plasmonic excitation and oxygen vacancy. *Appl. Catal. B Environ.* **2021**, *292*, 120147. [[CrossRef](#)]
43. Wang, Y.X.; Zhang, Y.Y.; Zhu, X.J.; Liu, Y.; Wu, Z.B. Fluorine-induced oxygen vacancies on TiO<sub>2</sub> nanosheets for photocatalytic indoor VOCs degradation. *Appl. Catal. B Environ.* **2022**, *316*, 121610. [[CrossRef](#)]
44. Santara, B.; Giri, P.K.; Imakita, K.; Fujii, M. Evidence of oxygen vacancy induced room temperature ferromagnetism in solvothermally synthesized undoped TiO<sub>2</sub> nanoribbons. *Nanoscale* **2013**, *5*, 5476–5488. [[CrossRef](#)] [[PubMed](#)]
45. Xiao, Z.; Ji, S.; Li, Y.; Hou, F.; Zhang, H.; Zhang, X.; Wang, L.; Li, G. Tuning oxygen vacancies on mesoporous ceria nanorods by metal doping: Controllable magnetic property. *Appl. Surf. Sci.* **2018**, *455*, 1037–1104. [[CrossRef](#)]
46. Chi, M.; Sun, X.; Sujun, A.; Davis, Z.; Tatarchuk, B.J. A quantitative XPS examination of UV induced surface modification of TiO<sub>2</sub> sorbents for the increased saturation capacity of sulfur heterocycles. *Fuel* **2019**, *238*, 446–454. [[CrossRef](#)]
47. Mao, D.L.; Jia, M.M.; Qiu, J.H.; Zhang, X.F.; Yao, J.F. N-Doped porous carbon supported Au nanoparticles for benzyl alcohol oxidation. *Catal. Lett.* **2019**, *150*, 74–81. [[CrossRef](#)]
48. Zhang, X.G.; Ke, X.B.; Zhu, H.Y. Zeolite-supported gold nanoparticles for selective photooxidation of aromatic alcohols under visible-light irradiation. *Chem. Eur. J.* **2012**, *18*, 8048–8056. [[CrossRef](#)]
49. Savara, A.; Rossetti, I.; Chan, C.E.T.; Prati, L.; Villa, A. Microkinetic modeling of benzyl alcohol oxidation on carbon-supported Palladium nanoparticles. *ChemCatChem* **2016**, *8*, 2482–2491. [[CrossRef](#)]
50. Zhu, Y.F.; Wei, Y.F. Solvent-controlled copper-catalyzed oxidation of benzylic alcohols to aldehydes and esters. *Eur. J. Org. Chem.* **2013**, *2013*, 4503–4508. [[CrossRef](#)]
51. Mao, D.L.; Qiu, J.H.; Jia, M.M.; Zhang, X.F.; Yao, J.F. Platinum supported cellulose-based carbon with oxygen-containing functional groups for benzyl alcohol oxidation. *J. Phys. Chem. Solids.* **2019**, *135*, 109095. [[CrossRef](#)]
52. Duarte, H.A.; Luggren, P.J.; Zelin, J.; Sad, M.E.; Díez, V.K.; Cosimo, J.I.D. Selective aerobic oxidation of benzyl alcohol on inexpensive and reusable ZnO/MnCO<sub>3</sub> catalysts. *Catal. Today* **2021**, *394–396*, 178–189. [[CrossRef](#)]
53. Manash, J.B.; Tonmoy, J.B.; Rupjyoti, D.; Subhasish, R.; Ankur Kanti, G.; Kusum, K.B. Fe(III) superoxide radicals in halloysite nanotubes for visible-light-assisted benzyl alcohol oxidation and oxidative CC coupling of 2-naphthol. *Mol. Catal.* **2021**, *515*, 111858.

54. Gogoi, G.; Nath, J.K.; Hoque, N.; Biswas, S.; Gour, N.K.; Kalita, D.J.; Bora, S.R.; Bania, K.K. Single and multiple site Cu(II) catalysts for benzyl alcohol and catechol oxidation reactions. *Appl. Catal. A Gen.* **2022**, *644*, 118816. [[CrossRef](#)]
55. Yang, D.J.; Liu, H.W.; Zheng, Z.F.; Yuan, Y.; Zhao, J.C.; Waclawik, E.R.; Ke, X.B.; Zhu, H.Y. An efficient photocatalyst structure: TiO<sub>2</sub>(B) nanofibers with a shell of anatase nanocrystals. *J. Am. Chem. Soc.* **2009**, *131*, 17885–17893. [[CrossRef](#)]
56. Aguilar Tapia, A.; Delannoy, L.; Louis, C.; Han, C.W.; Ortalan, V.; Zanella, R. Selective hydrogenation of 1,3-butadiene over bimetallic Au-Ni/TiO<sub>2</sub> catalysts prepared by deposition-precipitation with urea. *J. Catal.* **2016**, *344*, 515–523. [[CrossRef](#)]
57. Marques, J.; Gomes, T.D.; Forte, M.A.; Silva, R.F.; Tavares, C.J. A new route for the synthesis of highly-active N-doped TiO<sub>2</sub> nanoparticles for visible light photocatalysis using urea as nitrogen precursor. *Catal. Today* **2018**, *326*, 36–45. [[CrossRef](#)]
58. Zope, B.N.; Hibbitts, D.D.; Neurock, M.; Davis, R.J. Reactivity of the Gold/Water Interface During Selective Oxidation Catalysis. *Science* **2010**, *330*, 74–78. [[CrossRef](#)]
59. Skupien, E.; Berger, R.; Santos, V.; Gascon, J.; Makkee, M.; Kreutzer, M.; Kooyman, P.; Moulijn, J.; Kapteijn, F. Inhibition of a Gold-Based Catalyst in Benzyl Alcohol Oxidation: Understanding and Remediation. *Catalysts* **2014**, *4*, 89–115. [[CrossRef](#)]
60. Marianna, B.; Guillermo Escolano, C.; Leonardo, P.; Lorenzo, M. Surface processes in selective photocatalytic oxidation of hydroxybenzyl alcohols by TiO<sub>2</sub> P25. *Catal. Today* **2022**, *413–415*, 113983.
61. Zhang, X.G.; Durndell, L.J.; Isaacs, M.A.; Parlett, C.M.A.; Lee, A.F.; Wilson, K. Platinum-catalyzed aqueous-phase hydrogenation of d-glucose to d-sorbitol. *ACS Catal.* **2016**, *6*, 7409–7417. [[CrossRef](#)]

**Disclaimer/Publisher’s Note:** The statements, opinions and data contained in all publications are solely those of the individual author(s) and contributor(s) and not of MDPI and/or the editor(s). MDPI and/or the editor(s) disclaim responsibility for any injury to people or property resulting from any ideas, methods, instructions or products referred to in the content.